Available online at www.sciencedirect.com

ScienceDirect

Ceramics International 40 (2014) 1593–1598

CERAMICS INTERNATIONAL

www.elsevier.com/locate/ceramint

Study on the slag corrosion resistance of unfired Al_2O_3–SiC/β-Sialon/Ti(C, N)–C refractories

De-Xin Yang, Yan-Gai Liu*, Ming-Hao Fang, Zhao-Hui Huang, Ding-Yun Ye

School of Materials Science and Technology, China University of Geosciences (Beijing), Beijing 100083, PR China

Received 11 April 2013; received in revised form 9 July 2013; accepted 9 July 2013
Available online 16 July 2013

Abstract

Al_2O_3–SiC–C refractories are widely used in the steelmaking process due to their outstanding properties, and in order to improve their slag corrosion resistance, the erosion resistant materials have often been used. β-Sialon and Ti(C, N) are point out as novel additives that present suitable properties to increase the corrosion resistance of refractories. In this study, unfired Al_2O_3–SiC/β-Sialon/Ti(C, N)–C refractories were prepared using Ti(C, N)/β-Sialon powders, brown alumina, SiC, micro α-Al_2O_3 powder, silica fume, ball pitch, calcium aluminate cement, aluminum and silicon as the starting materials. The effect of the Ti(C, N)/β-Sialon powders and SiC on the slag penetration and corrosion resistance of the refractories was investigated, and the slag resistance mechanisms of the Al_2O_3–SiC/β-Sialon/Ti(C, N)–C refractories were also discussed. Fractal theory, scanning electron microscopy (SEM) and energy dispersive spectroscope (EDS) were carried out in order to better understand the slag resistance effects and reaction mechanisms. The results showed that all samples made with Ti(C, N)/β-Sialon powders had excellent slag corrosion resistance. The slag corrosion resistance of the samples was based on their low apparent porosity and high volume density. The β-Sialon and SiC powders contributed to the improved slag corrosion resistance performance of the composite refractories.

Keywords: Unfired refractories; Ti(C, N)/β-Sialon powders; Slag resistance; Fractal theory

1. Introduction

It is well known that the steel metallurgy industries need to consume abundant amounts of refractory material, including shaped and unshaped refractories [1–3]. This is, especially so in puddling blast furnace systems [4], including the process engineering of blast furnace shells, casting houses, and molten iron storage, and transportation, etc. [5,6]. These require numerous Al_2O_3–SiC–C refractories [7]. Although increases in the prices of the raw materials restricts the use of Al_2O_3–SiC–C castables in steelmaking plants, these unshaped refractories maintain their high consumption level due to their excellent thermal shock and slag corrosion resistance properties [8]. The Al_2O_3–SiC–C refractories are mainly fabricated using corundum, carborundum, micro α-Al_2O_3 powder, micro silica powder, and calcium aluminate cement as starting materials, which markedly improves the working life of the refractory materials used in blast furnace iron making systems. In addition, they provide the refractory conditions required for large scale production in blast furnaces [9].

The refractory castables used in the steel making industries typically comprise of a mixture of coarse (5–100 mm) and fine (100–0.1 mm) raw materials, a binding agent (e.g., calcium aluminate cement) and chemical additives in water [10]. Since the 1990s, unshaped refractories have seen a sharp increase using in steel-making applications [11]. In particular, refractory castables containing α-Al_2O_3, SiC and C are being used with increasing frequency [12]. However, corrosion caused by liquid oxides is one of the most severe modes of degradation which limits the lifetime of the refractory linings [13]. Consequently, carbon-containing [14] and carborundum-containing [15] refractory castables are widely used in blast furnaces due to their high refractoriness, thermal shock resistance, and low molten slag wettability [16–18]. These materials can improve the slag corrosion resistance of the refractories used in blast furnaces.

In this study, β-Sialon and Ti(C, N) powders were synthesized using the carbothermal reduction and nitridation (CRN)

*Corresponding author. Tel.: +86 10 82322186; fax: +86 10 82322186.
E-mail address: liuyang@cugb.edu.cn (Y.-G. Liu).

0272-8842/$ - see front matter © 2013 Elsevier Ltd and Techna Group S.r.l. All rights reserved.
http://dx.doi.org/10.1016/j.ceramint.2013.07.047

Table 1
Phase composition of the as-synthesized powders.

Specimen no.	Temperature/C	Major phase(s)		Minor phase
L1	1450	β-Sialon		15 R($SiAl_4O_2N_4$)
L2	1400	β-Sialon	Ti(C, N)	α-Al_2O_3
L3	1350	β-Sialon	Ti(C, N)	α-Al_2O_3
L4	1350	β-Sialon	Ti(C, N)	α-Al_2O_3

method which decreases prices by substitution of micro powders such as brown alumina (0.074 mm, 0.044 mm), 97SiC (0.074 mm), and micro α-Al_2O_3 powder (0.074 mm). This is because obtaining these micro powders consumes a great deal of energy. Beside this, β-Sialon can be used in many fields requiring elevated temperatures because of its superior corrosion resistance [19], hardness and flexure strength [20], and resistance to thermal shock [21]. Consequently, β-Sialon powder is a viable candidate for use in Al_2O_3–SiC–C castables and has the ability to improve the slag corrosion resistance of the refractories [22,23].

The Ti(C, N)/β-Sialon powders were synthesized in 3 h in a nitrogen atmosphere from low-grade bauxite and ilmenite raw materials using CRN at different temperatures (Table 1). According to Table 1, the main phase compositions of the as-synthesized powders were Ti(C, N) and β-Sialon after removing iron by washing with hydrochloric acid. The mechanism of the non-oxide phase composition Ti(C, N) and SiC/β-Sialon resistance to slag erosion was discussed in a later section.

2. Experimental procedures

The Ti(C, N)/β-Sialon powders were synthesized by CRN using different ratios of low-grade bauxite and ilmenite. The weight ratios used were 100:0, 90:10, 70:30 and 50:50, and the corresponding composite powders were labeled as L1, L2, L3 and L4. The iron in the Ti(C, N)/β-Sialon powders was removed by washing with hydrochloric acid.

Five types of unfired Al_2O_3–SiC/β-Sialon/Ti(C, N)–C refractories were designed corresponding to different types of Ti(C, N)/β-Sialon powders. The sample numbers of the unfired refractories were designated S1, S2, S3 and S4 corresponding to the additive Ti(C, N)/β-Sialon powders L1, L2, L3 and L4. Additionally, a sample S0, without Ti(C, N)/β-Sialon powders, was used as a control group.

The unfired Al_2O_3–SiC/Sialon/Ti(C, N)–C refractories with different types of Ti(C, N)/β-Sialon powders were produced using brown alumina (8–5 mm, 5–3 mm, 3–1 mm, 1–0 mm, 0.074 mm, 0.044 mm), 97SiC (0.074 mm), 90SiC (1–0 mm), micro α-Al_2O_3 powder (0.074 mm), silica fume (0.044 mm), ball pitch, calcium aluminate cement (CA-70), aluminum, and silicon as the starting materials, with sodium hexametaphosphate as additive.

The refractories were made using the static crucible method and fractal dimension calculations were used to discuss the results. In addition, according to the close stacking principle, the mass percentage of coarse particles (>1 mm) accounted for about 48 wt%; intermediate particles (1–0.088 mm) represented approximately 22 wt% and powders constituted around 30 wt% in the unfired refractories. Besides this, the mass fraction of Ti(C, N)/β-Sialon powders in this formulation was 5% and the proportion of the other raw materials was almost the same among samples S1, S2 and S3. As the purpose of the Ti(C, N)/β-Sialon powders was to substitute some of the micro powders, the percentages of brown alumina (0.074 mm, 0.044 mm), 97SiC (0.074 mm), micro α-Al_2O_3 powder (0.074 mm) in samples S1, S2 and S3 were less than those in S0.

Table 2
Chemical composition of blast furnace slag, (mass%).

CaO	SiO_2	Al_2O_3	MgO	Fe_2O_3	K_2O	TiO_2	others
35.85	30.90	17.23	10.56	0.70	0.55	0.45	3.76

The raw materials were initially mixed for 5 min in a mortar mill. Then they were mixed for 3 min after adding distilled water (approximately 7 wt% of the total mass). Prior to this, water reducer (sodium hexametaphosphate), which accounted for 3 wt‰ of the gross mass, was added to the water until it completely dissolved. Afterwards, crucible samples ($d=50$ mm and $h=50$ mm) were prepared in a crucible mold using 30 MPa pressure and an inner bore of ∅20 mm × 25 mm. The crucible samples were dried at room temperature for 24 h. Then they were cured at 110 °C for 24 h in a drying oven. After that, 6 g of blast furnace slag was put into the inner bore of the crucible samples filling about two-thirds of this volume. Subsequently, the crucible samples were sintered at 1450 °C for 3 h in a high temperature furnace with in an air atmosphere and the samples were then cut along the center line after natural cooling. The chemical composition of the blast furnace slag was shown in Table 2.

The micro-morphologies and micro-area chemical analysis of the products were examined by scanning electron microscopy (SEM; JEM-6460LV microscope, Japan) equipped with an energy dispersive spectroscopy (EDS, INCA X-sight, Oxford Instrument, UK).

3. Results and discussion

3.1. Slag corrosion resistance of the composite refractories

Photographs of the crucible section morphology after corrosion using blast-furnace slag at 1450 °C for 3 h in an air atmosphere were shown in Fig. 1. It can be seen from the photographs that all the five samples were only slightly eroded by the blast-furnace slag because most of the slag was residual and the slag blowholes had clear outlines. Furthermore, every boundary between slag and sample was distinct — the interior structure of the crucible was compact and the aggregate and the matrix were closely combined. It can be demonstrated that the specimens had excellent performance with respect to resistance to slag penetration and melting loss. However, the erosion reaction was serious on the three-phase border between the matrix, slag, and air, in which the apertures of the crucibles were enlarged. Moreover, the interior structures of the diameters in specimens S3 and S4 were expanded greater than in

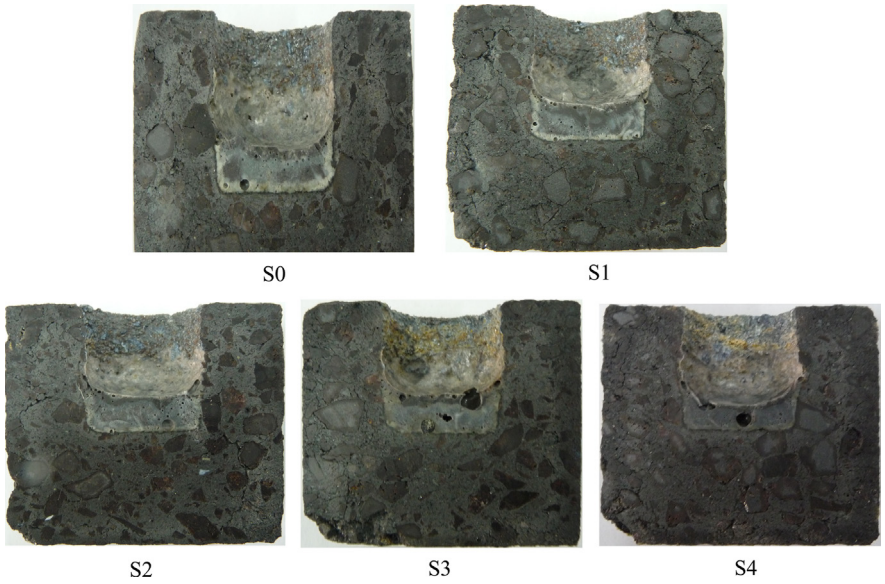

Fig. 1. Photographs of the crucible section morphology after slag erosion at 1450 °C for 3 h.

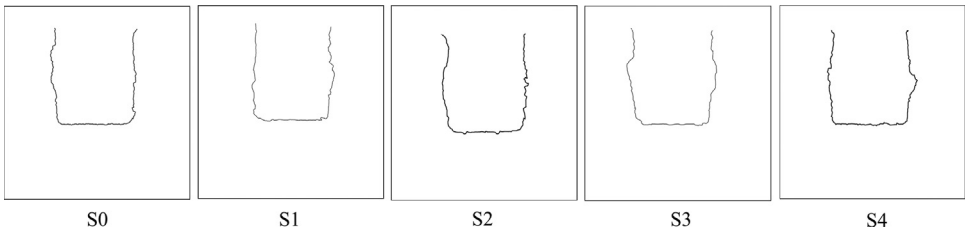

Fig. 2. The crucible boundary morphology for fractal dimension calculation.

the others and their outlines were also fuzzier. According to the quantity of residual melting slag which was slightly more in specimens S1 and S2 than the others, these specimens had better slag corrosion resistance performance than the others.

According to the discussion above, it may be concluded that Ti(C,N)/β-Sialon powders could effectively replace parts of the brown alumina (0.074 mm and 0.044 mm), 97SiC (0.074 mm), and α-Al_2O_3 micro powder (0.074 mm) used in Al_2O_3–SiC–C refractories.

However, the static crucible method cannot accurately illustrate the slag corrosion resistance performance in slag erosion experiments, because it is easy to add subjective ideas from the researchers involved. So, comparing and analyzing results from different researchers is difficult. In order to improve the objectivity and accuracy of this study, the fractal theory [24] is introduced to study the boundary shape of the specimens after eroding the composite refractories. For the refractory materials a clear concept, refractory fractal (Rf), is defined according to the definition of fractal dimension [24,25].

Rf=1: The aggregate and matrix of the refractory materials have the same corrosion resistance and the surface of the materials always remain smooth during erosion.

Rf=1.0–1.15: Refractory materials have excellent slag corrosion resistance and the boundary curve of the erosion surface primarily presents a smooth surface. Besides this, the residual safe thickness of the refractory materials can be estimated from theoretical values.

Rf=1.15–1.20: Refractory materials have moderate slag corrosion resistance and the boundary curve of the erosion surface is coarse. Moreover, the residual safe thickness of the refractory materials must be suitably magnified from the theoretical values.

Rf $\geq$ 1.20: Refractory materials have poor slag corrosion resistance and the boundary curve of the erosion surface presents an obvious undulating appearance. Furthermore, the residual safe thickness of the refractory materials cannot be estimated from the theoretical values.

Rf=2.0: The structures of the refractory materials are cracked and scattered after being affected by the erosion medium.

In this experiment, calculation of the fractal dimension of the erosion boundary morphology was carried out using the method of box counting. The values of the cell lengths, ε, used were 10, 20, 40, 60, 80 and 100 mm. The formulae for fractal dimension were as follows:

$$d_i = [\ln N(\varepsilon_0) - \ln N(\varepsilon_i)]/[\ln(\varepsilon_0) - \ln(\varepsilon_i)] \quad (1)$$

$$d = [\sum d_i]/n \quad (2)$$

where ε_0=10, ε_i=(20, 40, 60, 80 and 100), and n=5.

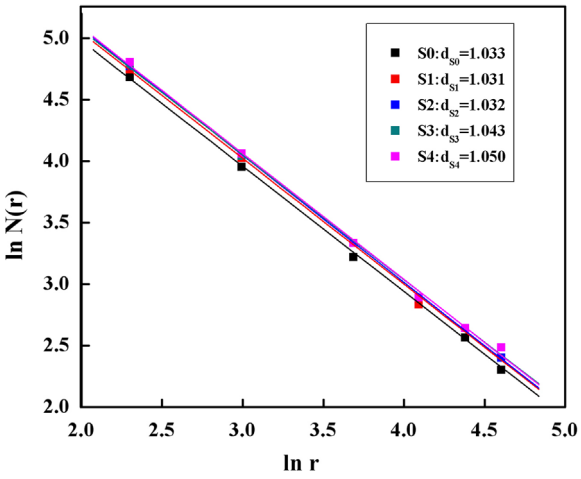

Fig. 3. Specimens from boundary fractal graphs.

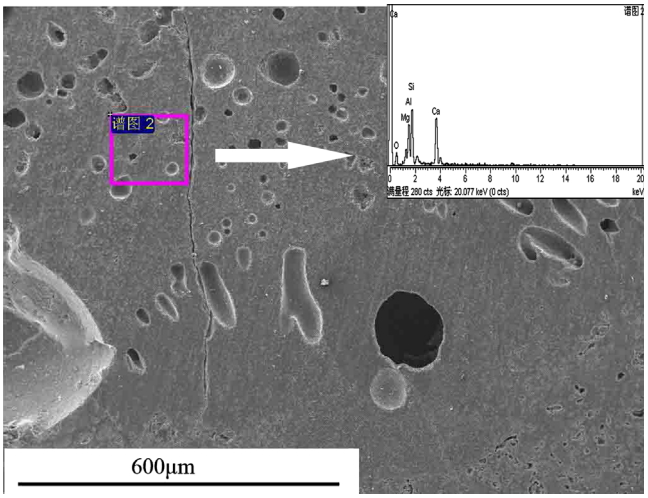

Fig. 4. Microstructure and EDS analysis of specimen S1 after slag erosion at 1450 °C for 3 h.

The crucible boundary morphology was shown in Fig. 2 for fractal dimension calculations corresponding to the photographs in Fig. 1.

The boundary fractal graphs were calculated (Fig. 3) from the crucible boundary morphology in Fig. 2 using the box counting method. Consequently, the fractal dimensions of the erosion boundaries in the specimens from various unfired Al_2O_3–SiC/β-Sialon/Ti(C, N)–C refractories were calculated after the slag erosion experiments. It is manifest from Fig. 3 that, according to the refractory fractal, the slag erosion resistance of the five specimens was excellent, and that there was no apparent distinction between the numerical values of the fractal dimensions of the slag corrosion resistance in the five specimens. More specifically, the numerical values of the fractal dimensions from the specimens S0, S1, and S2 were almost the same and slightly larger than those from S3 and S4. The results showed that the slag corrosion resistance of specimens S0, S1, and S2 were slightly better and the performance of S1 was the best.

In general, it had been shown that the slag corrosion resistance of the unfired Al_2O_3–SiC/β-Sialon/Ti(C, N)–C refractories was excellent with the Ti(C, N)/β-Sialon powders. Also, the slag corrosion resistance of the samples S1 and S2 was a little better than that of the control group S0. The conclusion was that the addition of Ti(C, N)/β-Sialon powders could improve the slag corrosion resistance of Al_2O_3–SiC–C refractories.

3.2. The microstructure of the composite refractories after slag erosion

The results of microstructure and energy dispersive spectroscopy (EDS) analyses on specimen S1 after slag erosion at 1450 °C for 3 h in air was shown in Fig. 4. According to the figure, the density of the melting slag was high after slag erosion but the melting slag also included numerous pores. After analyzing the EDS results from the melting slag, it was found that the melting slag mainly contained the elements Ca, Al, Si, Mg, and O, with corresponding percentages of 26.56%, 14.59%, 19.39%, 5.06%, and 34.41%.

The microstructure and line scanning on the specimen S0 after slag erosion at 1450 °C for 3 h were shown in Fig. 5. It was seen that the combination between the matrix and aggregate (brown alumina and SiC) was extremely tight and the coarse and fine aggregates were also closely packed, which formed a strong interface. These structures ensured that the Al_2O_3–SiC/β-Sialon/Ti(C, N)–C refractories had excellent usability.

Fig. 6 showed results from the conversion zone between the slag and crucible bottom and line scanning of sample S2 after slag erosion at 1450 °C for 3 h. Ca in the blast furnace slag was the main element invading the interior structure of the matrix. Consequently, the content of Ca in both the melting slag and matrix could be used to judge the level of matrix erosion by the melting slag. According to the line scanning in Fig. 6, it was obvious that the Ca content decreases continuously from the slag layer, penetration layer, to matrix and that the thickness of the penetration layer was approximately 0.5 mm. Table 3 gave the Ca content at points 1, 2, 3 and 4 of the sample S2 by EDS analysis. It illustrated that the content of Ca decreased rapidly from point 3, which demonstrated that the melting slag erosion did not reach up to point 3.

From the fractal dimension calculation results, the slag corrosion resistance of unfired Al_2O_3–SiC/β-Sialon/Ti(C, N)–C refractories was excellent and a discussion of the slag resistance mechanism follows.

Firstly, carbides and nitrides were not readily wetted by the melting slag, so the slag penetration was small in the refractories. These kinds of structures and compositions ensured the composite refractories having excellent performance in terms of resistance to melting slag erosion.

Furthermore, adding Ti(C, N)/β-Sialon powders were one of the key measures to improve the slag corrosion resistance of unfired Al_2O_3–SiC/β-Sialon/Ti(C, N)–C refractories. This was because β-Sialon had superior thermal properties, chemical

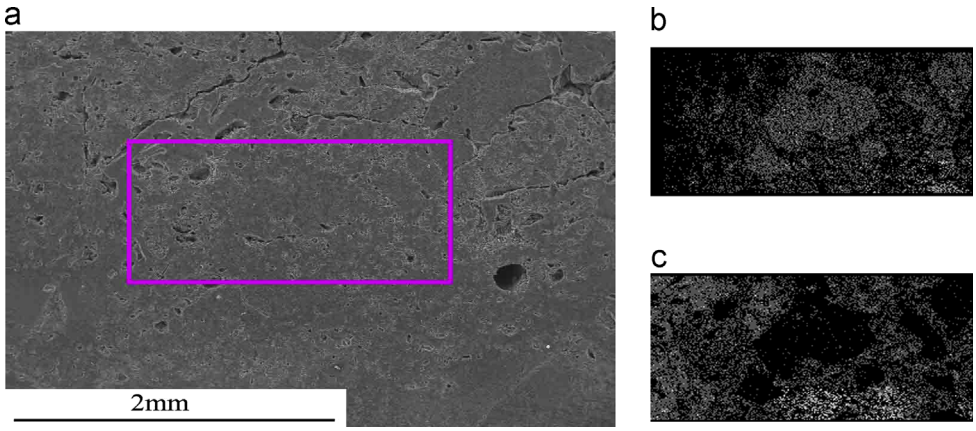

Fig. 5. Microstructure and line scanning on sample S0 after slag erosion at 1450 °C for 3 h. (a) The matrix of the sample So (b) Al element and (c) Si element.

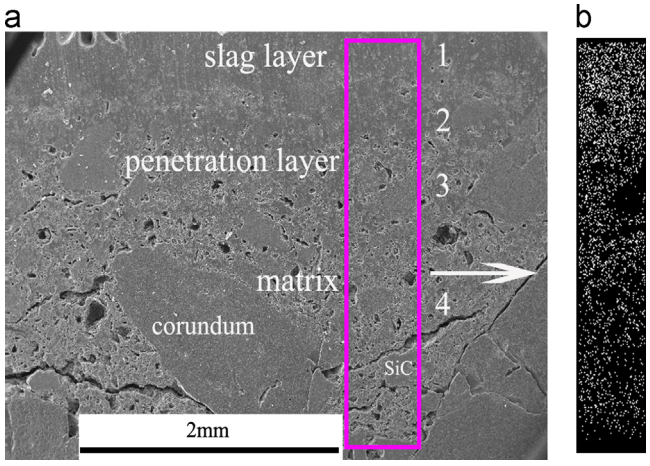

Fig. 6. Microstructure and line scanning on sample S2 after slag erosion at 1450 °C for 3 h. (a) The conversion zone between slag and crucible bottom and (b) Ca element.

Table 3
The elemental Ca content at different points in specimen S2, (wt%).

Point	1	2	3	4
Ca	20.87	16.35	3.73	1.81

stability, and an excellent resistance to slag erosion. Non-oxide SiC also had great slag corrosion resistance [26]. Therefore, β-Sialon and non-oxide SiC contributed greatly to promoting slag corrosion resistance in the composite refractories.

Lastly, Ti(C, N) and β-Sialon powders deposited in the reaction layer between melting slag and the matrix effectively prevented oxygen passing into the matrix of the composite refractories. Some raw materials also produced high silica glass phases that contained high viscosity N compounds, which also contributed to improve slag erosion resistance. Meanwhile, the wetting angle between Ti(C, N) and melting slag was small and this effectively resisted the melting slag eroding and infiltrating the matrix.

4. Conclusions

Generally, the slag erosion resistance of the unfired Al_2O_3–SiC/β-Sialon/Ti(C, N)–C refractories made was excellent according to the method of static crucible and fractal dimension calculation. Ti(C, N)/β-Sialon powders (specimen L1) were able to improve the slag corrosion resistance of the composite refractories. However, when the content of Ti(C, N) (such as specimens L2, L3, and L4) was excessive, they had negative effects on the slag erosion resistance of the re-prepared refractories.

The low porosity and high volume density of the unfired Al_2O_3–SiC/β-Sialon/Ti(C, N)–C refractories contribute to the slag corrosion resistance. In addition, β-Sialon and non-oxide SiC was also beneficial for improving the slag erosion resistance of the composite refractories.

Acknowledgments

This work was supported by the National Natural Science Foundation of China (Grant no. 51032007), the Fundamental Research Funds for the Central Universities (Grant nos. 2652012071 and 2652013040), the Key Projects in the National Science & Technology Pillar Program (Grant no. 2011BAB03B08), the Program for New Century Excellent Talents in University of Ministry of Education of China (Grant no. NCET-12–0951) and the Key Laboratory on Deep GeoDrilling Technology, Ministry of Land and Resources (Grant no. NLSD201216).

References

[1] O. Sasan, D. Arash, Microstructure and phase evolution of alumina-spinel self-flowing refractory castables containing nano-alumina particlesk, Ceramics International 37 (2011) 1003–1009.
[2] G.D.T. Angeles, J.V. Francisco, H.D.A. Antonio, Direct mineralogical composition of a MgO–C refractory material obtained by Rietveld methodology, Journal of The European Ceramic Society 26 (2006) 2587–2592.
[3] X.C. Li, B.Q. Zhu, T.X. Wang, Effect of electromagnetic field on slag corrosion resistance of low carbon MgO–C refractories, Ceramics International 38 (2012) 2105–2109.

[4] P. Nicolas, O. Evariste, High temperature mechanical characterisation of an alumina refractory concrete for blast furnace main trough Part I. General context, Journal of The European Ceramic Society 28 (2008) 2859–2865.
[5] W.S. Resende, R.M. Stoll, S.M. Justus, R.M. Andrade, E. Longo, J.B. Baldo, E.R. Leite, C.A. Paskocimas, L.E.B. Soledade, J.E. Gomes, J.A. Varela, Key features of alumina/magnesia/graphite refractories for steel ladle lining, Journal of The European Ceramic Society 20 (2000) 1419–1427.
[6] S. Mucahit, A. Sedat, O. Salih, A microstructural study of surface hydration on a magnesia refractory, Ceramics International 36 (2010) 1731–1735.
[7] O. Sasan, A.B. Mohammad, M. Fatollah, M. Fatollah, R.N. Mohammad, The effect of deflocculants on the self-flow characteristics of ultra low-cement castables in Al_2O_3–SiC–C system, Ceramics International 31 (2005) 647–653.
[8] M. Leonardo, M. Vanesa, H.L. Marcelo, G.T.M. Analı´a, High temperature mechanical behavior of Al_2O_3–MgO–C refractories for steelmaking use, Ceramics International 37 (2011) 1473–1483.
[9] A.P. Luz, V.C. Pandolfelli, Thermodynamic evaluation of SiC oxidation in Al_2O_3–$MgAl_2O_4$–SiC–C refractory castables, Ceramics International 36 (2010) 1863–1869.
[10] R.O. Ivone, R.S. Andre, A.O.V. Fernando, C.P. Victor, Setting behavior of ultra-low cement refractory castables in the presence of citrate and polymethacrylate salts, Journal of The European Ceramic Society 23 (2003) 2225–2235.
[11] R. L.A. D´ıaz, F. Torrecillas, G. Simonin, Fantozzi, Room temperature mechanical properties of high alumina refractory castables with spinel, periclase and dolomite additions, Journal of The European Ceramic Society 28 (2008) 2853–2858.
[12] X.L. Shi, Y. Tan, F.M. Xu, Y.L. Dong, Z.J. Zhang, X.N. Li, L. Wang, Mechanical properties of Al_2O_3–SiC–C composites using polycarbosilane as SiC precursor, Journal of Alloys and Compounds 490 (2012) 484–487.
[13] J. Poirier, F. Qafssaoui, J.P. Ildefonse, M.L. Bouchetou, Analysis and interpretation of refractory microstructures in studies of corrosion mechanisms by liquid oxides, Journal of The European Ceramic Society 28 (2008) 1557–1568.
[14] A.P. Luz, M.M. Miglioli, T.M. Souza, S. Hashimoto, S. Zhang, V.C. Pandolfelli, Effect of Al_4SiC_4 on the Al_2O_3–SiC–SiO_2–C refractory castables performance, Ceramics International 38 (2012) 3791–3800.
[15] M.F. Gazulla, M.P. G´omez, M. Orduña, A. Barba, Physico-chemical characterisation of silicon carbide refractories, Journal of The European Ceramic Society 26 (2006) 3451–3458.
[16] M. Chen, N. Wang, J.K. Yu, A. Yamaguchi, Oxidation protection of CaO–ZrO_2–C refractories by addition of SiC, Ceramics International 33 (2007) 1585–1589.
[17] S. Zhang, W.E. Lee, Influence of additives on corrosion resistance and corroded microstructures of MgO–C refractories, Journal of The European Ceramic Society 21 (2001) 2393–2405.
[18] P. Prigent, M.L. Bouchetou, J. Poirier, E. Bilbao, E. Blond, Corrosion of oxide bonded silicon carbide refractories by molten salts in solid waste-to-energy facilities, Ceramics International 38 (2012) 5643–5649.
[19] Y.T. Li, Z.H. Huang, Y.G. Xu, M.H. Fang, Y.G. Liu, J.Z. Yang, X.Z. Hu, Synthesis of ZrN-sialon composites from zircon and alumina by carbothermal reduction–nitridation, Materials Research Bulletin 47 (2012) 3272–3276.
[20] X.L. Sun, K.N. Sun, M. Du, W.L. Wang, A. Li, Effect of Al_2O_3 and Fe_3Al on the phase formation and mechanical properties of β-Sialon, Materials & Design 39 (2012) 373–378.
[21] G.M. Zheng, J. Zhao, C. Jia, X.H. Tian, Y.W. Dong, Y.H. Zhou, Thermal shock and thermal fatigue resistance of Sialon-Si_3N_4 graded composite ceramic materials, International Journal of Refractory Metals & Hard Materials 35 (2012) 55–61.
[22] G.H. Liu, K.X. Chen, J.T. Li, Growth mechanism of crystalline SiAlON microtubes prepared by combustion synthesis, Crystengcomm 14 (2012) 5585–5588.
[23] Z.Y. Mao, Y.C. Zhu, L. Gan, Y. Zeng, F.F. Xu, Y. Wang, H. Tian, D.J. Wang, SiALON-based crystal–glass composite phosphor with tunable yellow–green–blue color emission induced by SiO_2 melting corrosion, Journal of Materials Chemistry 22 (2012) 1983.
[24] B.B. Mandelbrot, J.W. Van ness, Fractional Brownian motions, fractional noises and application, Siam Review 10 (1968) 422–437.
[25] J.G. Hou, Z.Q. Wu, α-Ge/Au Double membrane after annealing of fractal formation, Acta Physica Sinica 37 (1988) 1735.
[26] H.J. Zhang, B. Han, Z.J. Liu, Preparation and oxidation of bauxite based β-Sialon-bonded SiC composite, Materials Research Bulletin 41 (2006) 1681–1689.